Materials Advances

ROYAL SOCIETY OF CHEMISTRY

PAPER

View Article Online
View Journal | View Issue

Cite this: *Mater. Adv.*, 2026, 7, 3690

Nano-assembly and cytotoxicity of the L-valine–polyamine conjugates of betulinic acid

Martina Wimmerová,[a] Miroslav Šlouf,[b] Marie Kvasnicová,[cd] Lucie Rárová,[c] David Šaman[e] and Zdeněk Wimmer*[a]

Six target derivatives of betulinic acid with several L-valine–polyamine conjugates were synthesized as a part of a series of 15 new compounds. The structures of all target compounds and their intermediates were elucidated by standard analytical methods. The target compounds were subjected to transmission electron microscopy (TEM) to prove their ability to form nano-assemblies in methanol and in water and to cytotoxicity assays in two cancer cell lines, cervical cancer (HeLa) and breast adenocarcinoma (MCF7), using normal human fibroblasts (BJ) as reference cells for determining the cytotoxicity of the investigated compounds. For detailed TEM studies, the target compounds (**6**, **7**, **11**, **12**, **16** and **17**) were dissolved in methanol and in water, and their nano-assemblies were observed after the application of the microscale fast-solvent removal protocol. All compounds were found to form various combinations of three basic morphologies: (i) isometric nanoparticles with the size ranging from 10 to 100 nm, (ii) long nanofibres with a thickness below 10 nm, and (iii) thin amorphous films upon fast-solvent removal. The fibrous morphologies were often located around the isometric nanoparticles and tended to grow with time. The nano-assemblies formed in methanol were often different from those formed in water, but the above-mentioned three basic morphologies (nanoparticles, nanofibres, and thin amorphous films) could be observed reproducibly for each compound. The target compounds showed cytotoxicity in the cancer cell lines, and regrettably, in non-malignant cells as well. Compounds **12** and **17** displayed the highest cytotoxicity against the HeLa cancer cell line among the synthesized compounds. Compound **12** also showed the highest cytotoxicity against the MCF7 cancer cell line. The effect of a dynamic self-assembly process on cytotoxicity was investigated in all target compounds. All of the studied compounds showed a better cytotoxicity profile against the HeLa cancer cell line than cisplatin, a pharmacologically used anticancer agent. This effect was less pronounced in the MCF7 cancer cell line and in normal human fibroblasts.

Received 6th November 2025,
Accepted 19th February 2026

DOI: 10.1039/d5ma01285f

rsc.li/materials-advances

1. Introduction

A series of 15 amide derivatives of betulinic acid bearing diamine skeletons, combined with the L-valine unit in the six target compounds, were designed and synthesized. The target compounds were investigated for their nano-assembly characteristics and cytotoxic effects.

Betulinic acid, (3β)-3-hydroxylup-20(29)-en-28-oic acid (**1**; Scheme 1), a pentacyclic triterpenoid of the lupane family, was used in this investigation. Biological activities and other characteristics of betulinic acid and its numerous derivatives have already been described and reviewed several times.[1–3]

The polyamines used as the structural modifiers of betulinic acid (**1**) are generally organic compounds often applied as convenient building blocks in designing novel biologically active compounds.[4–6] Diamines used in this investigation are considered to be a part of the group of polyamines. Ethylene diamine has been used during the design of several common drugs.[7] Piperazine and its simple derivatives have been used as anti-parasitic drugs. Piperazine has been used in functional antidepressants, antipsychotics, antihistamines, antifungals, antibiotics, urologicals and serotonin antagonists, acting at serotonin (5-HT) receptors.[8,9] The piperazine motif has appeared in cytotoxic drugs as well.[10,11] It has also been present in compounds acting as topoisomerase I inhibitors.[12] Homopiperazine (1,4-diazacycloheptane; 1,4-diazepane) has also often been a part of biologically active compounds.[13,14]

L-Valine, (2*S*)-2-amino-3-methylbutanoic acid, is an essential amino acid in animals. Its degradation is impaired in several

[a] *University of Chemistry and Technology in Prague, Department of Chemistry of Natural Compounds, CZ-16628 Prague, Czech Republic*
[b] *Institute of Macromolecular Chemistry, Czech Academy of Sciences, CZ-16206 Prague, Czech Republic*
[c] *Laboratory of Growth Regulators, Faculty of Science, Palacký University & Institute of Experimental Botany, Czech Academy of Sciences, CZ-77900 Olomouc, Czech Republic*
[d] *Department of Experimental Biology, Faculty of Science, Palacký University, CZ-77900 Olomouc, Czech Republic*
[e] *Institute of Organic Chemistry and Biochemistry, Czech Academy of Sciences, CZ-16610 Prague, Czech Republic*

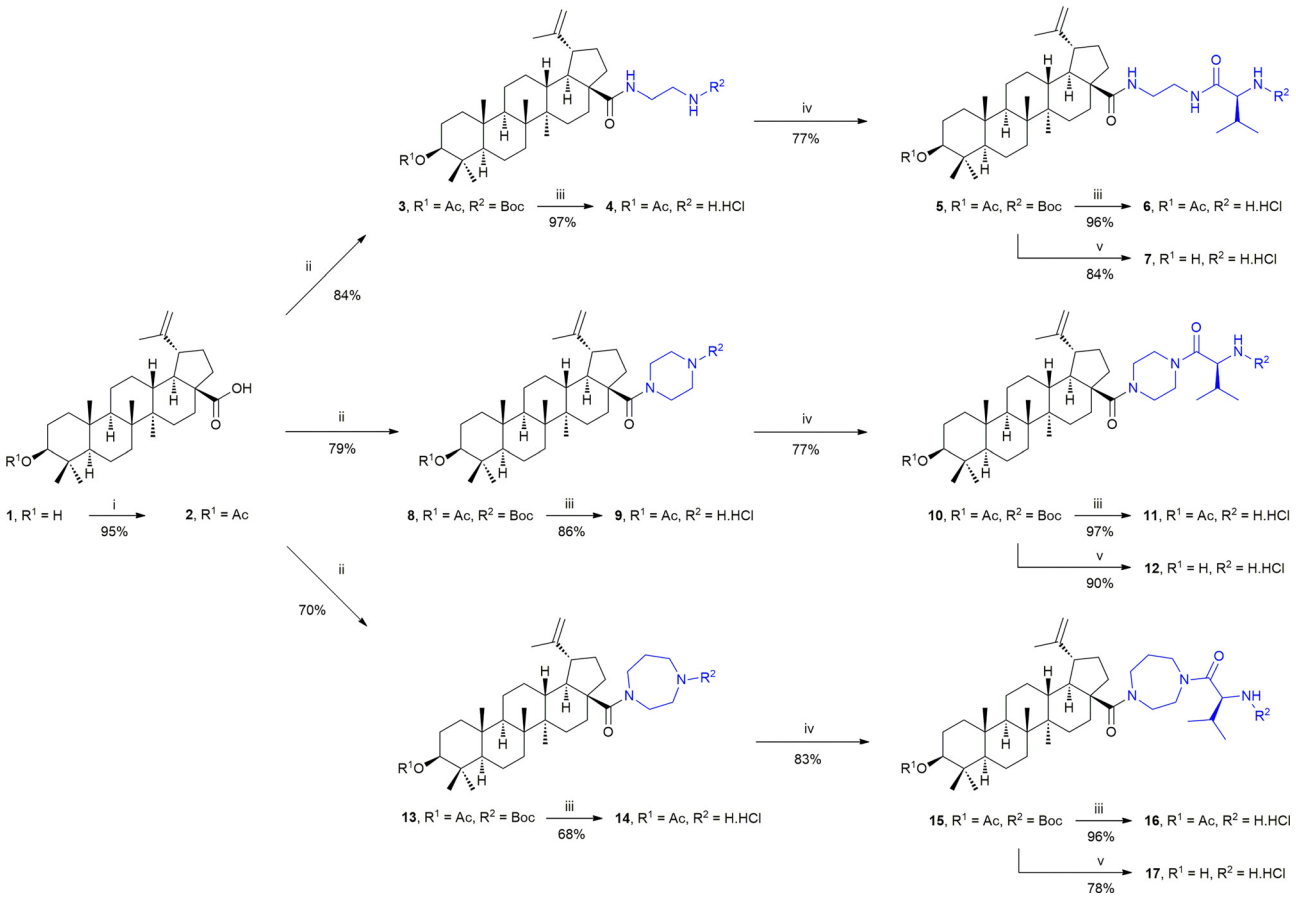

Scheme 1 Synthetic procedures: (i) acetic anhydride, DIPEA, DMAP, and THF; (ii) (a) oxalyl chloride, DCM; (b) *N*-Boc protected diamine, DIPEA, DCM, argon atmosphere; (iii) HCl (gas) in 1,4-dioxane; (iv) Boc-L-valine, EDC·HCl, HOBt, NMM, DCM, argon atmosphere; (v) (a) $LiOH{\cdot}H_2O$, methanol; (b) HCl (gas) in 1,4-dioxane.

metabolic diseases.[15] Lower levels of serum L-valine, like other branched-chain amino acids, are associated with weight loss and decreased insulin resistance: higher levels of L-valine were observed in the blood of diabetic mice, rats, and humans.[16]

The objectives of the present investigation are as follows: (a) to design and synthesise a series of derivatives of betulinic acid bearing ethylene diamine, piperazine and homopiperazine units as part of their molecules; (b) to modify their structures subsequently by introducing the L-valine unit; (c) to study the nano-assembly characteristics and the cytotoxicity of the target compounds; and (d) to study the potential relationships between the ability of the target compounds to form nano-assemblies and their cytotoxicity.

2. Experimental

2.1. General

The NMR measurements were performed on a Bruker AVANCE II 600 MHz spectrometer equipped with a 5 mm TCI cryoprobe in a 5 mm tube in different solvents. The ^{1}H NMR and the ^{13}C NMR spectra were recorded at 600.13 MHz and 150.90 MHz (AVANCE II 600 MHz) in $CDCl_3$ (at 293 K) or in DMSO-d_6 (at 373 K) using tetramethylsilane (δ = 0.0 – $CDCl_3$) or the signal of the solvent (δ = 2.50 or 39.50 for ^{1}H/^{13}C – DMSO-d_6) as internal references. The ^{1}H NMR data are presented in the following order: chemical shifts (δ) expressed in ppm, multiplicity (s, singlet; d, doublet; t, triplet; q, quartet; m, multiplet), number of protons, and coupling constants in Hertz. For unambiguous assignment of both ^{1}H and ^{13}C signals, the 2D NMR ^{1}H,^{13}C gHSQC and gHMBC spectra were measured using standard parameter sets and pulse programs supplied by the manufacturer of the spectrometer. Infrared spectra (IR) were measured with a Nicolet iS5 FT-IR spectrometer. Mass spectra (MS) were measured with a Waters ZMD mass spectrometer, mostly in a positive ESI mode (coin voltage, CV = 10 to 20 eV). Transmission electron microscopy (TEM) images were obtained with a Tecnai G2 Spirit Twin 12 microscope (FEI, Brno, Czech Republic). TLC was carried out on silica gel plates (Merck 60F_{254}) and visualization was performed by both, UV detection and spraying with a methanolic solution of phosphomolybdic acid (5%) followed by heating. For column chromatography, silica gel 60 (0.063–0.200 mm) from Merck was used. All chemicals and solvents were purchased from regular commercial sources in analytical grade and the solvents were purified by general methods before use. Triterpenoids were purchased from Dr

Jan Šarek – Betulinines (https://www.betulinines.com). All analytical data, *i.e.*, the evaluated ^{1}H and ^{13}C NMR spectra, IR and MS spectra, elemental analyses, the scanned NMR spectra of the prepared compounds, and the calculated ^{1}H and ^{13}C NMR spectra (ChemBioDraw Ultra, version 12.0) are presented in the SI, Experimental part, Fig. S1–S26.

2.2. Synthetic procedures

2.2.1. (3β)-3-(Acetyloxy)lup-20(29)-en-28-oic acid (2). Acetic anhydride (0.6 mL; 6.35 mmol) was added to a solution of **1** (2.02 g; 4.33 mmol), DIPEA (2 mL; 11.6 mmol) and DMAP (80 mg; 0.66 mmol) in dry THF (10 mL) under an argon atmosphere. The mixture was heated to 95 °C for 3 h. After cooling the mixture to r.t., water was added and the mixture was allowed to stand at r.t. overnight, and then extracted with chloroform. The extract was dried over sodium sulphate, the solid was filtered off, the solvent was evaporated under reduced pressure, and the residue was purified by column chromatography on silica gel using a chloroform/methanol mixture (100 : 1 to 50 : 1) as the mobile phase, affording **2** (2.09 g) in a 95% yield.

2.2.2. (3β)-28-({2-[(*tert*-Butoxycarbonyl)amino]ethyl}amino)-28-oxolup-20(29)-en-3-yl acetate (3). Oxalyl chloride (6.5 mL; 13.0 mmol) was added to a solution of **2** (0.93 g; 1.86 mmol) in dry DCM (15 mL) under an argon atmosphere, and the mixture was stirred at r.t. for 3 h. The solvent was evaporated under reduced pressure, and the crude product was dissolved in dry DCM. Boc-protected ethylene diamine (0.35 mL; 2.24 mmol) and DIPEA (0.88 mL; 4.84 mmol) were added to the above solution, and the resulting mixture was stirred at r.t. overnight. The solvent was evaporated under reduced pressure, and the residue was purified by column chromatography on silica gel using a chloroform/methanol (100 : 1) mixture as the mobile phase, affording **3** (0.997 g) in an 84% yield.

2.2.3. (3β)-28-[(2-Aminoethyl)amino]-28-oxolup-20(29)-en-3-yl acetate (4). A solution of HCl (gas; 4 M; 4 mL; 16 mmol) in 1,4-dioxane was added to a solution of **3** (0.997 g; 1.56 mmol) in 1,4-dioxane (12 mL), and the mixture was stirred at r.t. overnight. The solvent was evaporated under reduced pressure, and the residue was purified by column chromatography on silica gel using a chloroform/methanol (10 : 1 to 1 : 1) mixture as the mobile phase, affording **4** (0.82 g) in a 97% yield.

2.2.4. (3β)-28-[(2-{[((*N*-(*tert*-Butoxycarbonyl)-(2*S*)-2-amino-3-methylbutanoyl)amino)ethyl]amino}-28-oxolup-20(29)-en-3-yl acetate (5). A solution of Boc-L-valine (0.36 g; 1.67 mmol) in dry DCM (5 mL) was added to a solution of **4** (0.897 g; 1.63 mmol), HOBt (0.27 g; 2.0 mmol), and NMM (0.41 g; 4.03 mmol) in dry DCM (15 mL). After stirring the mixture for 30 min, EDC·HCl (0.487 g; 2.54 mmol) was added, and the resulting mixture was stirred at r.t. for 12 h. The reaction mixture was quenched with brine, and the organic phase was extracted with chloroform. After drying the extract over sodium sulphate, the solid was filtered off through a sintered glass funnel, and the solvent was evaporated under reduced pressure. The residue was purified by column chromatography on silica gel using a chloroform/methanol (98 : 2) mixture as the mobile phase, affording **5** (0.97 g) in a 77% yield.

2.2.5. (3β)-28-Oxo-28-{[((2-(2*S*)-2-amino-3-methylbutanoyl)-amino)ethyl]amino}lup-20(29)-en-3-yl acetate (6). Using the identical synthetic procedure as described for the preparation of **4**, product **6** (0.22 g) was obtained in a 96% yield.

2.2.6. (3β)-3-Hydroxy-(*N*-{[(2-(2*S*)-2-amino-3-methylbutanoyl)-amino]ethyl}lup-20(29)-en-28-amide (7). LiOH·H_2O (0.102 g; 2.43 mmol) was added to a solution of **5** (0.333 g; 0.45 mmol) in methanol (20 mL), and the mixture was heated under reflux for 4 h. The solvent was evaporated under reduced pressure, and the crude residue was treated with HCl (gas) in 1,4-dioxane as described above for the preparation of **4**. After purification of the product by column chromatography, **7** (0.24 g) was obtained in an 84% yield.

2.2.7. *tert*-Butyl 4-[(3β)-3-acetyloxy-28-oxolup-20(29)-en-28-yl]piperazin-1-carboxylate (8). Using the identical synthetic procedure as described for the preparation of **3**, product **8** (0.681 g) was obtained in a 79% yield.

2.2.8. (3β)-28-Oxo-28-(piperazin-1-yl)lup-20(29)en-3-yl acetate (9). Using the identical synthetic procedure as described for the preparation of **4**, product **9** (0.296 g) was obtained in an 86% yield.

2.2.9. (3β)-28-{4-[(*N*-(*tert*-Butoxycarbonyl)-(2*S*)-2-amino-3-methylbutanoyl]piperazin-1-yl}-28-oxolup-20(29)-en-3-yl acetate (10). Using the identical synthetic procedure as described for the preparation of **5**, product **10** (0.3 g) was obtained in a 77% yield.

2.2.10. (3β)-28-Oxo-28-{[(4-(2*S*)-2-Amino-3-methylbutanoyl)-piperazin-1-yl]lup-20(29)-en-3-yl} acetate (11). Using the identical synthetic procedure as described for the preparation of **4**, product **11** (0.11 g) was obtained in a 97% yield.

2.2.11. (3β)-28-{4[(2*S*)-2-Amino-3-methylbutanoyl]piperazin-1-yl}-3-hydroxylup-20(29)-en-28-one (12). Using the identical synthetic procedure as described for the preparation of **7**, product **12** (0.1 g) was obtained in a 90% yield.

2.2.12. *tert*-Butyl 4-[(3β)-3-(acetyloxy)-28-oxolup-20(29)-en-28-yl]-1,4-diazepane-1-carboxylate (13). Using the identical synthetic procedure as described for the preparation of **3**, product **13** (0.613 g) was obtained in a 70% yield.

2.2.13. (3β)-28-(1,4-Diazepan-1-yl)-28-oxolup-20(29)-en-3-yl acetate (14). Using the identical synthetic procedure as described for the preparation of **4**, product **14** (0.3 g) was obtained in a 68% yield.

2.2.14. (3β)-3-28-{4-[*N*-(*tert*-Butoxycarbonyl)-(2*S*)-2-amino-3-methylbutanoyl]-1,4-diazepan-1-yl}-28-oxolup-20(29)-en-3-yl acetate (15). Using the identical synthetic procedure as described for the preparation of **5**, product **15** (0.297 g) was obtained in an 83% yield.

2.2.15. (3β)-28-Oxo-28-{[(2*S*)-2-amino-3-methylbutanoyl]-1,4-diazepan-1-yl}lup-20(29)-en-3-yl acetate (16). Using the identical synthetic procedure as described for the preparation of **4**, product **16** (0.107 g) was obtained in a 96% yield.

2.2.16. (3β)-28-{4-[(2*S*)-2-Amino-3-methylbutanoyl]-1,4-diazepan-1-yl}-3-hydroxolup-20(29)-en-28-one (17). Using the identical synthetic procedure as described for the preparation of **7**, product **17** (0.11 g) was obtained in a 78% yield.

2.3. Transmission electron microscopy

The general procedure for the sample preparation and collection of micrographs was described in full detail recently.[5] Briefly, the samples were prepared by a microscale fast-solvent removal method as follows: each compound was dissolved in methanol and in water, each solution (2 μL) was dropped onto a standard TEM copper grid covered with a thin, electron-transparent carbon film, left to equilibrate for 1 min, and the excess solvent was removed by touching the bottom of the grid with a thin strip of filter paper. In this way, the solvent (2 μL) is removed instantly, the nano-assemblies are fixed on the film, and can be observed by TEM as documented in numerous previous studies.[17–19] In this work, all TEM micrographs were obtained with a Tecnai G2 Spirit Twin microscope (FEI, Czech Republic) using bright field imaging at an accelerating voltage of 120 kV.

2.4. Cell culture and cytotoxicity screening tests

The human cancer cell lines used in this investigation included cervical carcinoma (HeLa) and breast adenocarcinoma (MCF7) from the European Collection of Authenticated Cell Cultures (Salisbury, UK). Human foreskin fibroblasts (BJ) were used as reference cells (ATCC, Manassas, Virginia, USA). The process of cell culturing and their maintenance was also described in full detail recently.[5] The cytotoxicity screening tests were performed according to the standard experimental procedure.[4,20]

3. Results and discussion

3.1. Synthetic procedures and NMR measurements

The synthetic procedure is shown in Scheme 1. Because the research team has been dealing with the synthesis of various derivatives of different triterpenoids for a long time, several synthetic steps described below have already been applied in the synthesis of different substrates before.[21,22] Thus, **1** was converted into **2** using acetic anhydride in THF in the presence of a base (DIPEA) and a reaction accelerator (DMAP) to protect the free hydroxyl group in **1** before performing the following reaction step on the C(17)-COOH group (path i). The subsequent reaction steps are analogous with all three used diamines. In the former step, the new amide bond was formed in two steps (path ii), using a conversion of **2** into its acyl chloride by reacting **2** with oxalyl chloride in DCM. The crude acyl chloride of **2** was then reacted with the mono-Boc-protected diamine in DCM, using DIPEA as a base in the latter step, under an argon atmosphere, to afford the intermediate products **3**, **8** or **13**. Subsequently, the Boc protecting groups were removed from the respective compounds **3**, **8** or **13** using a 4 M solution of HCl (gas) in 1,4-dioxane, yielding the respective products **4**, **9** and **14** (path iii). The additional amide bond was formed by reacting the respective compounds **4**, **9** or **14** with the Boc-protected L-valine (path iv). The reagents, 1-hydroxybenzotriazol (HOBt) and *N*-methylmorpholine (NMM), were added to the above solution of the respective components in DCM, and left to stir for 30 min. Then the base, *N*-ethyl-*N*′-(3-dimethylaminopropyl)carbodiimide hydrochloride (EDC·HCl), was added under an argon atmosphere, and the reaction mixture was left to stir for several hours (path iv). Finally, the respective products **5**, **10** and **15** were obtained. The target compounds should form two subseries, either bearing the C(3)-OAc group (**6**, **11** and **16**; path iii) or bearing the C(3)-OH group (**7**, **12** and **17**; path v) to prepare the required compounds for the nano-assembly and the cytotoxicity studies. Compounds **6**, **11** and **16** were prepared by removing the Boc-protecting group from **5**, **10** and **15**, as described above (path iii). Compounds **7**, **12** and **17** were prepared from **5**, **10** and **15** by the two-step procedure (path v). The former step consisted of liberating the C(3)-OH group from its acetate by lithium hydroxide in methanol, and the latter step consisted of removing the Boc-protecting group by the already applied action of a 4 M solution of HCl (gas) in 1,4-dioxane.

During the measurement of the NMR spectra of compounds **13–17** bearing the homopiperazine cycle in their molecules, it was found that the interpretation of the presence of the homopiperazine cycle and the L-valine unit in the spectra measured in $CDCl_3$ at 293 K is almost impossible due to the strong steric hindrance of this part of the molecules. However, measuring the NMR spectra of these compounds in DMSO-d_6 at 373 K resulted in the NMR spectra showing acceptable resolution for their evaluation. The *in silico* 3D-modelling of the structures **4**, **6**, **7**, **9**, **11**, **12**, **14**, **16** and **17** shows these molecules from different angles of view, and may contribute to a better imaging and a better understanding of the steric hindrance in the individual molecules (*cf.* SI, Fig. S27–S35).

3.2. Transmission electron microscopy (TEM)

The studied target compounds **6**, **7**, **11**, **12**, **16** and **17** were soluble both in methanol and in water, which makes them potentially attractive for pharmacological and biomedical applications. Their nano-assemblies in both solvents were studied by TEM after applying our microscale fast-solvent removal preparation protocol. The TEM micrographs showed three characteristic morphologies: (i) isometric nanoparticles with sizes ranging from 10 to 100 nm, (ii) long nanofibres with diameters below 10 nm, and (iii) amorphous thin films (Fig. 1–3). Compound **6** (Fig. 1a–1d) showed all three morphologies: in methanol, it formed soft hairy nanofibres that were observed at both 1 h and 48 h after dissolution (Fig. 1a and b). In water, compound **6** showed isometric nanoparticles combined with a thin amorphous film in the form of a grey amorphous background that seemed to be a system of not fully developed fibrous structures (Fig. 1c and d). Compound **7** showed nice soft hairy fibres in methanol located around solid nano-sized centres (20–50 nm) at 1 h after the preparation of the sample (Fig. 1e). The micrographs differed from those shown for **6**. When the imaging of **7** was made at a time of 48 h after the preparation of the samples, the solid centres were less pronounced, while the fibres did not change (Fig. 1f). When the samples of **7** were prepared in water, isometric nanoparticles (50–100 nm) were observed 1 h after the preparation of the sample (Fig. 1g). The images of the samples of **7** changed after 48 h, when the isometric nanoparticles were much less numerous while fibrous nanostructures appeared in their place

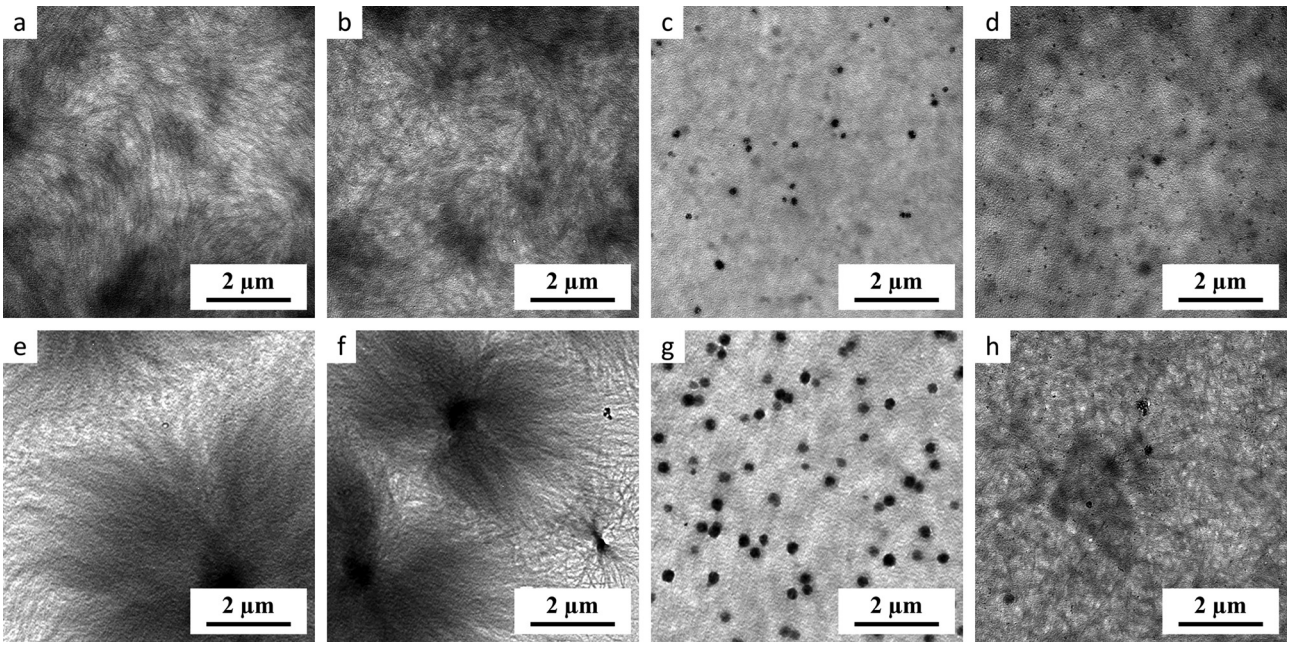

Fig. 1 Formation of nano-assemblies of **6** and **7** in methanol and in water. Legend: (a) **6** in methanol, 1 h; (b) **6** in methanol, 48 h; (c) **6** in water, 1 h; (d) **6** in water, 48 h; (e) **7** in methanol, 1 h; (f) **7** in methanol, 48 h; (g) **7** in water, 1 h; (h) **7** in water, 48 h.

(Fig. 1h). This supported our assumption that the amorphous structures tend to change into nanofibres in the course of time. Compound **11** (Fig. 2a–d) showed numerous isometric nanoparticles (50–100 nm) at a time of 1 h after the preparation of the sample in methanol (Fig. 2a). The number of these isometric nanoparticles increased and their size became more uniform (~200 nm) 48 h after the preparation of the sample, and they were accompanied by the fibrous nanomaterial (Fig. 2b). Much smaller isometric nanoparticles were found in water at both 1 h and 48 h after the preparation of the samples (Fig. 2c and d). Compound **12** (Fig. 2e–h) showed isometric nanoparticles (~200 nm) 1 h after the preparation of the sample in methanol (Fig. 2e). After 48 h, this developed into a fibrous nanomaterial, in which fibres were located around the central isometric

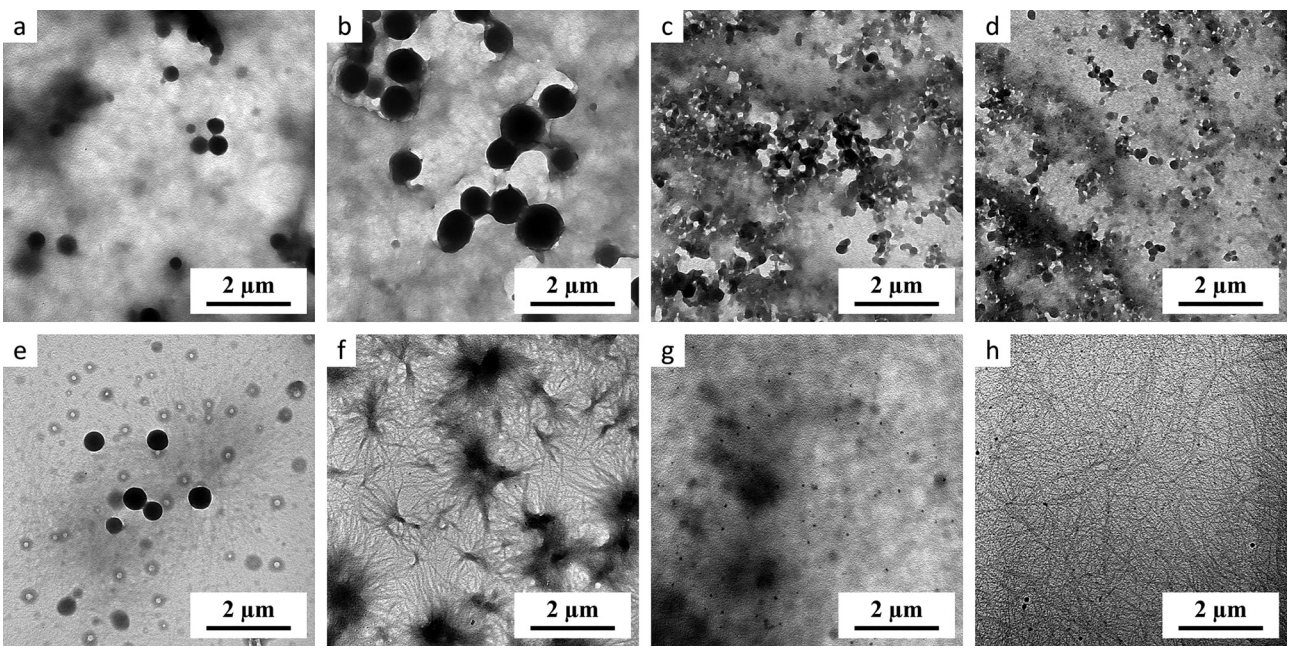

Fig. 2 Formation of nano-assemblies of **11** and **12** in methanol and in water. Legend: (a) **11** in methanol, 1 h; (b) **11** in methanol, 48 h; (c) **11** in water, 1 h; (d) **11** in water, 48 h; (e) **12** in methanol, 1 h; (f) **12** in methanol, 48 h; (g) **12** in water, 1 h; (h) **12** in water, 48 h.

nanoparticles of uneven shape (Fig. 2f). In water, compound **12** showed isometric nanoparticles (5–10 nm) accompanied by a small quantity of the fibrous nanomaterial 1 h after the preparation of the sample (Fig. 2g). The image changed again after 48 h, when mainly fibrous nanomaterial was observed together with still small isometric nanoparticles (5–10 nm; Fig. 2h). Compound **16** (Fig. 3a–d) showed clusters of isometric nanoparticles of uneven shape and a gel present in methanol 1 h after the preparation of the sample (Fig. 3a). The image changed completely after 48 h, when a combination of the isometric nanoparticles with the fibrous nanomaterial was observed (Fig. 3b). In water, **16** formed isometric nanoparticles (30–100 nm) surrounded by a thin amorphous film in the form of a dark grey background, with very few fibrous nanostructures observed after 1 h (Fig. 3c). However, the quantity of the fibrous nanomaterial increased substantially after 48 h, while the size of the isometric nanoparticles decreased (<10 nm; Fig. 3d). Compound **17** (Fig. 3e–h) showed behaviour analogous to **16**, by forming clusters of the isometric nanoparticles in methanol after 1 h (Fig. 3e) that were transformed into a mixture of the fibrous nanomaterial with the isometric nanoparticles after 48 h (Fig. 3f). In water, **17** formed isometric nanoparticles (10–30 nm) combined with the soft fibrous nanomaterial 1 h after the preparation of the sample (Fig. 3g). After 48 h, the image showed a much better pronounced fibrous nanomaterial combined with the unchanged isometric nanoparticles (Fig. 3h).

3.3. Cytotoxicity assays and their relationship to the nano-assembly

The target compounds **6**, **7**, **11**, **12**, **16** and **17** were subjected to screening tests for cytotoxicity in the two cancer cell lines, cervical cancer (HeLa) and breast adenocarcinoma (MCF7). Normal human fibroblasts (BJ) were used as the reference non-malignant cells. In addition, a pharmacologically applied anticancer agent, cisplatin (*cis*-diamminedichloroplatinum(ii); **CDDP**) was used to compare the results achieved with **6**, **7**, **11**, **12**, **16** and **17** with those of the clinically used agent (Table 1).

Compound **12** displayed the highest cytotoxicity among the studied compounds of this series in both cancer cell lines, HeLa and MCF7. Compound **17** displayed a comparable cytotoxicity with that of **12** in the HeLa cancer cell line. All compounds of this series showed higher cytotoxicity against the HeLa cancer cell line than cisplatin (**CDDP**). In turn, only **12** was slightly more cytotoxic against the MCF7 cancer cell line than **CDDP**. A great disadvantage of the compounds **6**, **7**, **11**, **12**, **16** and **17** was their high cytotoxicity in the human fibroblasts (BJ). The parent betulinic acid (**1**) showed no cytotoxicity ($IC_{50} > 50$ μM).

All compounds subjected to the cytotoxicity assay also displayed nano-assembly characteristics. Based on our results, these compounds are capable of forming nano-assemblies in the stock solutions of the studied compounds prepared for cytotoxicity assays. Table S1 (SI) summarizes the IC_{50} values obtained in the experimental repetitions (4 to 6 for each compound) of the cytotoxicity assays. The results presented therein show that cytotoxicity increased for most of the studied compounds with increasing time since the moment when the stock solutions were prepared before being used in the cytotoxicity assays. The data indicate that a dynamic self-assembly process took place in the stock solutions of the studied compounds and affected their measured cytotoxicity. Changes in the TEM images were also observed, and even if these two types of systems (TEM imaging and the cytotoxicity assay) cannot be directly compared, a hypothesis can be presented on the

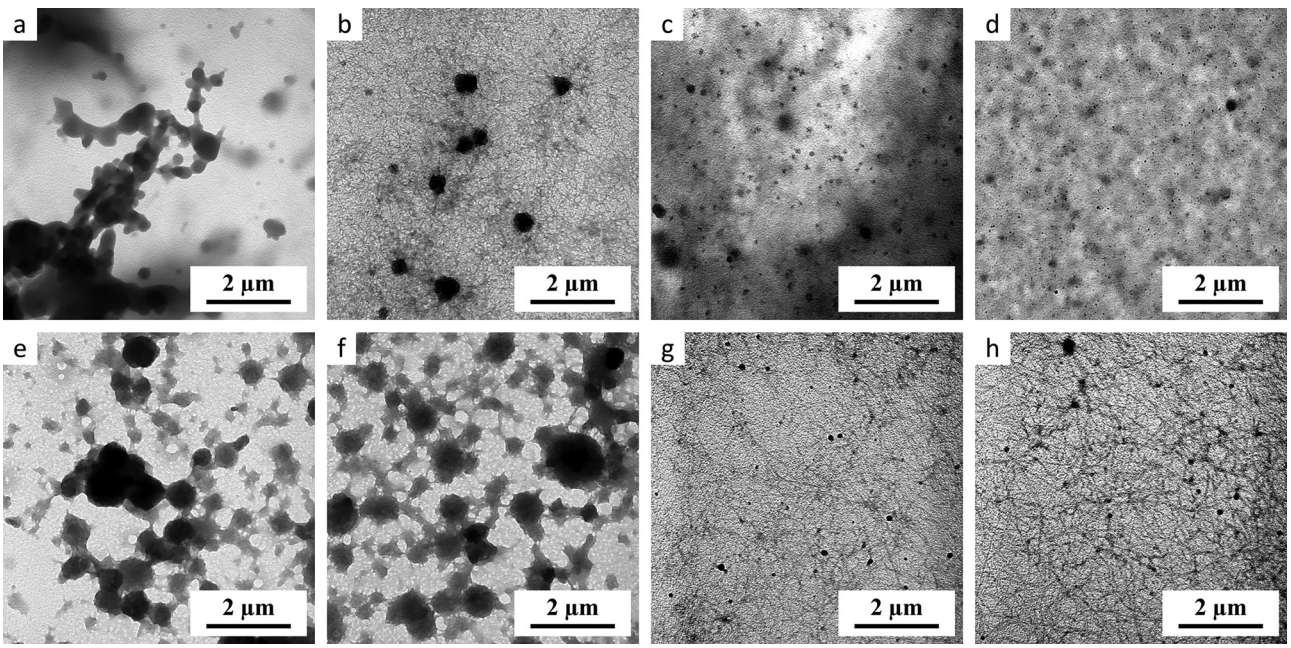

Fig. 3 Formation of nano-assemblies of **16** and **17** in methanol and in water. Legend: (a) **16** in methanol, 1 h; (b) **16** in methanol, 48 h; (c) **16** in water, 1 h; (d) **16** in water, 48 h; (e) **17** in methanol, 1 h; (f) **17** in methanol, 48 h; (g) **17** in water, 1 h; (h) **17** in water, 48 h.

Table 1 Cytotoxicity (IC_{50} ± SD [μM]) of the studied compounds in the two cancer cell lines and normal cells after 72 h of exposure

	IC_{50} ± SD [μM]		
Compound	HeLa[a]	MCF7[b]	BJ[c]
1	>50	>50	>50
6	8.51 ± 0.44	13.82 ± 0.21	7.88 ± 0.32
7	6.32 ± 1.98	12.65 ± 0.87	12.30 ± 1.80
11	7.33 ± 0.55	12.85 ± 0.29	11.27 ± 0.38
12	3.68 ± 0.86	4.09 ± 0.46	5.49 ± 1.28
16	7.66 ± 0.65	9.02 ± 1.04	10.35 ± 0.87
17	3.65 ± 0.25	10.25 ± 0.78	4.61 ± 0.94
CDDP	11.4 ± 3.8	7.7 ± 1.7	6.9 ± 0.9

[a] HeLa, cervical cancer. [b] MCF7, breast adenocarcinoma. [c] BJ, normal human fibroblasts.

formation of nano-assemblies during the cytotoxicity assays. This type of behaviour was observed in both tested cancer cell lines, as well as in normal human fibroblasts (SI, Table S1). The hypothesis assists in explaining the differences in the IC_{50} values of each studied compound in different repetitions of the biological experiments (SI, Table S1).

A similar behaviour of the triterpenoid derivatives has previously been observed in cytotoxicity assays.[4,5,23] Therefore, it seems to be likely that a relationship may exist between cytotoxicity and the ability of the studied compounds to self-assemble under the given conditions. Their biological activity is dependent on a dynamic self-assembly process, even if no direct evidence capable of proving the above presented hypothesis has been obtained during this investigation. Nevertheless, the advantages of nanomaterials in biomedical applications have already been observed and/or reviewed by other research teams as well.[24–27] The targeted formation of nanomaterials often resulted in augmenting the biological effects of the drugs, and nanomaterials are understood to represent convenient prodrugs.[4,27]

4. Conclusions

A series of 15 derivatives of betulinic acid were synthesized. Six compounds of this series were the target compounds subjected to the investigation of their ability to self-assemble into nanostructures and to the investigation of their potential cytotoxicity. Potential relationships between the formation of the nanostructures and the cytotoxicity of the target compounds were also studied. TEM imaging has evidenced that all target compounds formed nanostructures both in methanol and in water at 1 h and 48 h after the dissolution and the preparation of the samples for TEM imaging. Compound **6** formed soft hairy fibres in methanol within 1 h, and the images did not change over time. In water, **6** formed isometric nanoparticles combined with a thin amorphous film that seems to be a system of not fully developed fibrous structures at 1h and 48 h after the preparation of the sample. Compound **7** formed soft fibres located around solid centres only in methanol after 1 h. The solid centres appeared to be less pronounced over time. In water, compound **7** formed the isometric nanoparticles after 1 h, which became less pronounced after 48 h, when the fibrous nanostructures appeared. Compounds **11** and **12** formed isometric nanoparticles of different sizes both in methanol and in water after 1 h. They were later accompanied by the formation of fibrous nanostructures that became more visible in the micrographs of compound **12**. Compounds **16** and **17** formed isometric nanoparticles and/or their clusters both in methanol and in water after 1 h. Later on, fibrous nanostructures appeared in compound **17**, while isometric nanoparticles started to be less pronounced in compound **16** but remained unchanged in compound **17**.

When the TEM images of the nano-assemblies of the target compounds are compared with the results of the cytotoxicity assays presented in Table S1 (SI), it is clearly visible that nano-assembly affected the cytotoxicity of most of the target compounds. Most of the target compounds showed no cytotoxicity when freshly prepared solutions were applied to the cancer cells. In turn, the cytotoxicity for the target cells increased over time. The same effect appeared when the target compounds were tested in normal human fibroblasts. It is difficult to get irrefutable evidence for this hypothesis, because preparation of the samples for TEM imaging and the cytotoxicity assays required different approaches due to which the results are not comparable.

The effect of the controlled nano-assembly on the biological activity of small organic molecules still needs an intensive investigation to fully understand the relationships, which may contribute significantly to our understanding of the application of these compounds capable of nano-assembling in pharmacological and medicinal practice.

Author contributions

The manuscript was written through the contributions of all authors. All authors have given approval to the final version of the manuscript. Conceptualization: Z. W., M. Š., and L. R.; methodology: M. W., and M. K.; investigation: M. W., M. K., and D. Š.; resources: Z. W., L. R., and M. Š.; data curation: M. W., M. Š., and D. Š.; writing – original draft preparation: M. W., M. Š., L. R., D. Š., and Z. W.; writing – review and editing: M. Š., L. R., and Z. W.; project administration: M. Š., L. R., and Z. W.; funding acquisition: M. Š., L. R., and Z. W.

Conflicts of interest

There are no conflicts to declare.

Data availability

Data for this article are available from the corresponding author (Z. Wimmer) upon a request made at wimmerz@vscht.cz.

The data supporting this article have been included as a part of the supplementary information (SI). Supplementary information: the evaluated ^{1}H and ^{13}C NMR spectra, IR and MS spectra, elemental analyses, the scanned NMR spectra of the prepared compounds, the calculated ^{1}H and ^{13}C NMR spectra, the 3D-structures of several target compounds (ChemBioDraw Ultra, version 12.0), and the cytotoxicity data obtained in the

individual repetitions of the experiments. See DOI: https://doi.org/10.1039/d5ma01285f.

Acknowledgements

A part of this investigation was funded by the Specific University Research Grant No. A1_FPBT_2025_009. The microscopy study at the Institute of Macromolecular Chemistry was supported by the grant TN02000020 (TAČR). The authors thank Ms Jiřina Hromádková and Ms Tereza Štenclová for their excellent technical assistance.

References

1 Z. Özdemir and Z. Wimmer, *Phytochemistry*, 2022, **203**, 113340.
2 U. Bildziukevich, M. Wimmerová and Z. Wimmer, *Pharmaceuticals*, 2023, **16**, 386.
3 M. Wimmerová, U. Bildziukevich and Z. Wimmer, *Molecules*, 2023, **28**, 7718.
4 U. Bildziukevich, M. Malík, Z. Özdemir, L. Rárová, L. Janovská, M. Šlouf, D. Šaman, J. Šarek, Nonappa and Z. Wimmer, *J. Mater. Chem. B*, 2020, **8**, 484–491.
5 U. Bildziukevich, M. Šlouf, L. Rárová, D. Šaman and Z. Wimmer, *Soft Matter*, 2023, **19**, 7625–7634.
6 L. Černá, U. Bildziukevich, L. Rárová, J. Trylčová, D. Šaman, J. Weber, P. Lovecká and Z. Wimmer, *React. Chem. Eng.*, 2024, **9**, 1087–1095.
7 J. A. Bender, N. A. Meanwell and T. Wang, *Tetrahedron*, 2002, **58**, 3111–3128.
8 R. Kant and S. Maji, *Dalton Trans.*, 2021, **50**, 785–800.
9 F. Han, R. Yan, M. Zhang, Z. Xiang, Q. Wu and J. Li, *Nat. Prod. Res.*, 2020, **34**, 1282–1287.
10 Z. Özdemir, D. Šaman, K. Bertula, M. Lahtinen, L. Bednárová, M. Pazderková, L. Rárová, Nonappa and Z. Wimmer, *Langmuir*, 2021, **37**, 2693–2706.
11 Z. Özdemir, Nonappa and Z. Wimmer, *ACS Appl. Nano Mater.*, 2022, **5**, 16264–16277.
12 A. Talukdar, A. Kundu, D. Sarkar, S. Goon and M. Mondal, *Eur. J. Med. Chem.*, 2022, **236**, 114304.
13 N. A. Meanwell and O. Loiseleur, *J. Agric. Food Chem.*, 2022, **70**, 10942–10971.
14 N. A. Meanwell and O. Loiseleur, *J. Agric. Food Chem.*, 2022, **70**, 10972–11004.
15 A. Salazar, M. Keusgen and J. von Hagen, *Amino Acids*, 2016, **48**, 1161–1171.
16 C. J. Lynch and S. H. Adams, *Nat. Rev. Endocrinol.*, 2014, **10**, 723–736.
17 Z. Černochová, V. Lobaz, L. Čtveráčková, P. Černoch, M. Šlouf, M. Filipová, M. Hrubý and J. Pánek, *Eur. Polym. J.*, 2023, **190**, 111996.
18 S. Pytlíková, R. Konefal, R. Pola, A. Braunová, V. Lobaz, M. Šlouf, H. Beneš, D. Starenko, K. Běhalová, M. Kovář, T. Etrych, R. Laga and M. Pechar, *ACS Appl. Bio Mater.*, 2025, **8**, 271–284.
19 K. Kolouchova, N. Pien, F. N. Cetin, Z. Cernochova, J. Van Meerssche, M. Slouf, A.-A.-A. Bara, O. Groborz, M. Hruby and S. Van Vlierberghe, *Nanoscale*, 2025, **17**, 18709–18726.
20 L. Rárová, Z. Pakulski, M. Strnad, M. Kvasnicová, T. Štenclová and P. Cmoch, *J. Steroid Biochem. Mol. Biol.*, 2022, **224**, 106161.
21 U. Bildziukevich, L. Rárová, D. Šaman and Z. Wimmer, *Eur. J. Med. Chem.*, 2018, **145**, 41–50.
22 U. Bildziukevich, M. Kvasnicová, D. Šaman, L. Rárová, M. Šlouf and Z. Wimmer, *ACS Omega*, 2025, **10**, 20938–20948.
23 U. Bildziukevich, Z. Özdemir, D. Šaman, M. Vlk, M. Šlouf, L. Rárová and Z. Wimmer, *Org. Biomol. Chem.*, 2022, **20**, 8157–8163.
24 O. Jurček, S. Chattopadhyay, E. Kalenius, J. M. Linnanto, A. Kiesilä, P. Jurček, P. Radiměřský and R. Marek, *Angew. Chem., Int. Ed.*, 2024, **63**, e202409134.
25 P. Gomez-Romero, A. Pokhriyal, D. Rueda-Garcia, L. N. Bengoa and R. M. Gonzalez-Gil, *Chem. Mater.*, 2024, **36**, 8–27.
26 A. T. Chitakunye, O. C. Ezekiel, Q. Liu, S. Zhang and L. Cai, *J. Mater. Chem. B*, 2025, **13**, 11102–11125.
27 X. Zhang, S. Liu, R. Xin, W. Hu, Q. Zhang, Q. Lu and L. Han, *Mater. Horiz.*, 2025, **12**, 5749–5761.